RBRH

Revista Brasileira de Recursos Hídricos
Brazilian Journal of Water Resources
Versão On-line ISSN 2318-0331
RBRH, Porto Alegre, v. 27, e20, 2022
Scientific/Technical Article

https://doi.org/10.1590/2318-0331.272220220021

Effects caused by obstacles in the hydrodynamics of turbidity currents: an experimental approach

Efeitos causados por obstáculos na hidrodinâmica de correntes de turbidez: uma abordagem experimental

Arthur Costa Cerqueira[1] & Rafael Manica[1]

[1]Universidade Federal do Rio Grande do Sul, Porto Alegre, RS, Brasil
E-mails: arthurcosta.c@gmail.com (ACC), manica@iph.ufrgs.br (RM)

Received: March 16, 2022 - Revised: June 14, 2022 - Accepted: July 07, 2022

ABSTRACT

This research aims to evaluate the effects of the presence of obstacles on turbidity currents hydrodynamics. Nine physical simulations of a poorly sorted mixture of water and coal (Cvol = 5%; D50 = 47 μm) were run in a laboratory test channel with three flow discharges (5, 10 and 15 L.min^{-1}) in three different topographic configurations: runs without obstacles; runs with three 3 cm-high obstacles and runs with three 6 cm-high obstacles. The results showed that greater height of obstacles leads to greater blockage of the flow, causing changes on vertical profiles of velocity shape, flow regime (supercritical to subcritical), geometry and flow circulation in the zone between obstacles. Obstacle height reduction by 50% led to similar behavior of the turbidity current as the no-obstacles condition. After passing over the sequence of the obstacle, the turbidity current tended to regenerate a hydrodynamic structure comparable to the no-obstacles conditions.

Keywords: Physical modeling; Sediment gravity flow; Topographic obstacles.

RESUMO

Esta pesquisa visa avaliar os efeitos da presença de obstáculos na hidrodinâmica das correntes de turbidez. Nove simulações físicas de uma mistura mal selecionada de água e carvão (Cvol = 5%; D50 = 47 μm) foram executadas em um canal de acrílico medindo 4.00 x 0.49 x 0.24 m. Foram utilizadas três vazões de injeção (5, 10 e 25 L.min^{-1}) em três configurações topográficas diferentes: canal sem obstáculos, canal com três obstáculos de 3 cm de altura e canal com três obstáculos de 6 cm de altura. Os resultados mostraram que quanto maior a altura dos obstáculos, maior o bloqueio do escoamento, causando alterações nos perfis verticais da forma, da velocidade, do regime de escoamento (supercrítico para subcrítico), da geometria e da zona de recirculação entre os obstáculos. A redução da altura em 50% (3 cm) indica que a corrente de turbidez desenvolveu um comportamento semelhante à condição sem obstáculos. Após ultrapassar a sequência de obstáculos, o escoamento tende a regenerar sua própria estrutura hidrodinâmica da mesma forma que a condição imediatamente anterior aos obstáculos.

Palavras-chave: Modelagem física; Fluxo gravitacional de sedimento; Obstáculos topográficos.

INTRODUCTION

Density currents are a relative movement between two or more fluids of different densities, generating mixing interfaces (Simpson, 1969). Typically, these currents are composed of dissolved substances (temperature difference or salinity difference) and by suspended particles (Alavian, 1986).

Middleton & Hampton (1973) states that turbidity currents are a most common type of sediment gravity flow among the sedimentary processes in oceanic basins, because their initiation is linked to slope instability and bed remobilization. The interaction between sedimentary grains, turbulence, suspension and sediment mixing results in a phenomenon that has intrinsic hydraulic characteristic (Kneller & Buckee, 2000).

The two main parameters used to characterize turbidity currents are the velocity and the concentration profile. Current velocity and sediment concentration are parameters that respond to flow conditions and, therefore, express the hydrodynamic behavior of turbidity currents in space and over time (Altinakar et al., 1996; Mulder & Alexander, 2001; Manica, 2009).

The velocity profile of a turbidity current is divided into two regions: above and below the maximum velocity of the profile (Kneller & Buckee, 2000). Below maximum velocity, a region presents a positive-gradient exponential shape, whereas above a region presents a negative logarithmic shape (Altinakar et al., 1996; Manica, 2009).

The turbidity currents that flow into the ocean basins interact with the bed and topographic features of the sea floor, including salt diapirs, seamounts, volcanic islands and depressions (Wynn et al., 2000; Gee et al., 2001). These features become obstacles and cause resistance to the flow, blocking either totally or partially the flow, either confining or unconfining the transported sediment load. Furthermore, the hydraulic response of this interaction can be recorded in the generated deposits (Gee et al., 2001; Kneller & Buckee, 2000; Morris & Alexander, 2003; Patacci et al., 2015; Cumberpatch et al., 2021). Obstacles also deflect turbidity currents, causing them to follow different trajectories (Gee et al., 2001). These effects are more significant for higher obstacles and for concentrations of fine particles. Then, a partial blocking of the turbidity current occurs and a return current analogous to a translation wave is generated (Bursik & Woods, 2000; Kubo, 2004). Pari et al. (2010) observed that obstacles with a height between 2 and 2.75 times the height of the turbidity current can generate total blockage of the current. The effects of the obstacle are reduced as the density Froude number is increased, because there is sufficient inertial energy to be transformed into potential energy, *i.e.*, to overcome the obstacles. Flows with a densimetric Froude number less than one (subcritical) present a lower energy and overcome this topographical resistance (Kneller & Buckee, 2000; Pari et al., 2010; Oshaghi et al., 2013). When the obstacles are positioned in sequence, a recirculation may occur (Yaghoubi et al., 2017). Recirculation does not appear to be a static and permanent phenomenon, and is strongly influenced by the concentration of particles in the flow (Tokyay et al., 2011; Yaghoubi et al., 2017).

Understanding how turbidity currents interact with the ocean floor helps the description of regions where there will be hydrodynamics changes, deposition and remobilization of substrate in the field. However, monitoring is sometimes made difficult by the magnitude of these events (Gee et al., 2001). Due to this natural restraint, the experimental approach in the laboratory is an auxiliary tool to understand this natural process. Manica (2012) stated that physical modeling under controlled conditions allows the direct evaluation of the hydrodynamics and sediment transport currents.

Thus, this work aims to experimentally evaluate the effects of the presence of obstacles in the hydrodynamics of turbidity currents. Three different discharge runs passed above three identical obstacles with isosceles triangle shapes at two different heights of obstacles. The results are compared with a similar series of runs without obstacles. The objective is to understand the hydrodynamic interaction of the turbidity current with the bottom obstacles.

EXPERIMENTAL SETUP

The turbidity currents experimental runs were carried out at NECOD-IPH-UFRGS laboratory. A simulation acrylic channel was used, measuring 4.00 x 0.49 x 0.24 m and installed inside another external constant-level tank (Figure 1). An auxiliary reservoir (4 m-high) fed by gravity into the channel a mixture of water and sediment through a pipe and an electromagnetic flow meter (Siemens).

Nine physical simulations were performed, containing a mixture of water (ρ_A = 998 kg m^{-3}) and coal (ρ_s = 1140 kg. m^{-3}) at volumetric concentration of (Cvol) 5%, poorly selected and median (D50) = 47 μm. Three discharges were applied (5, 10 and 25 L.min^{-1}) in three different topographic situations: Series 1 - control runs without obstacles; Series 2 - runs with three 3 cm-high obstacles with isosceles triangles shapes; Series 3 - runs with three 6 cm-high obstacles with isosceles triangles shapes. The three obstacles were installed at 220 cm, 270 cm and 320 cm from the injection point.

To characterize and evaluate the flow properties, five UVP – ultrasonic velocity profiler device – were positioned at 45º and 40 cm above the floor (Koller, 2020) and at 105 cm, 190 cm (before obstacles), 260 (between obstacles), 320, and at 370 cm (after obstacles) from the injection point. In addition, a video camera GoPro® was positioned inside an external tank, laterally to the channel (by the first obstacle) to register the turbidity current development.

The experiments consisted of the continuous injection of 100 liters of water and sediment mixtures into the channel through a diffuser. Before and after the experiments, sediment mixture were sampled to calculate the bulk volumetric concentration of the mixture injected. The flow meter recorded the discharge and volume. Then, the UVP and the video-camera recorded the data of current passage along the entire channel. After the injection finished, the tank remained still for a couple of hours and then the external tank was slowly drained to avoid remobilization of the generated deposit (not evaluated here).

RESULTS

For all runs, the discharge measured with the magnetic flow rate had high correlation with the predicted value (Table 1).

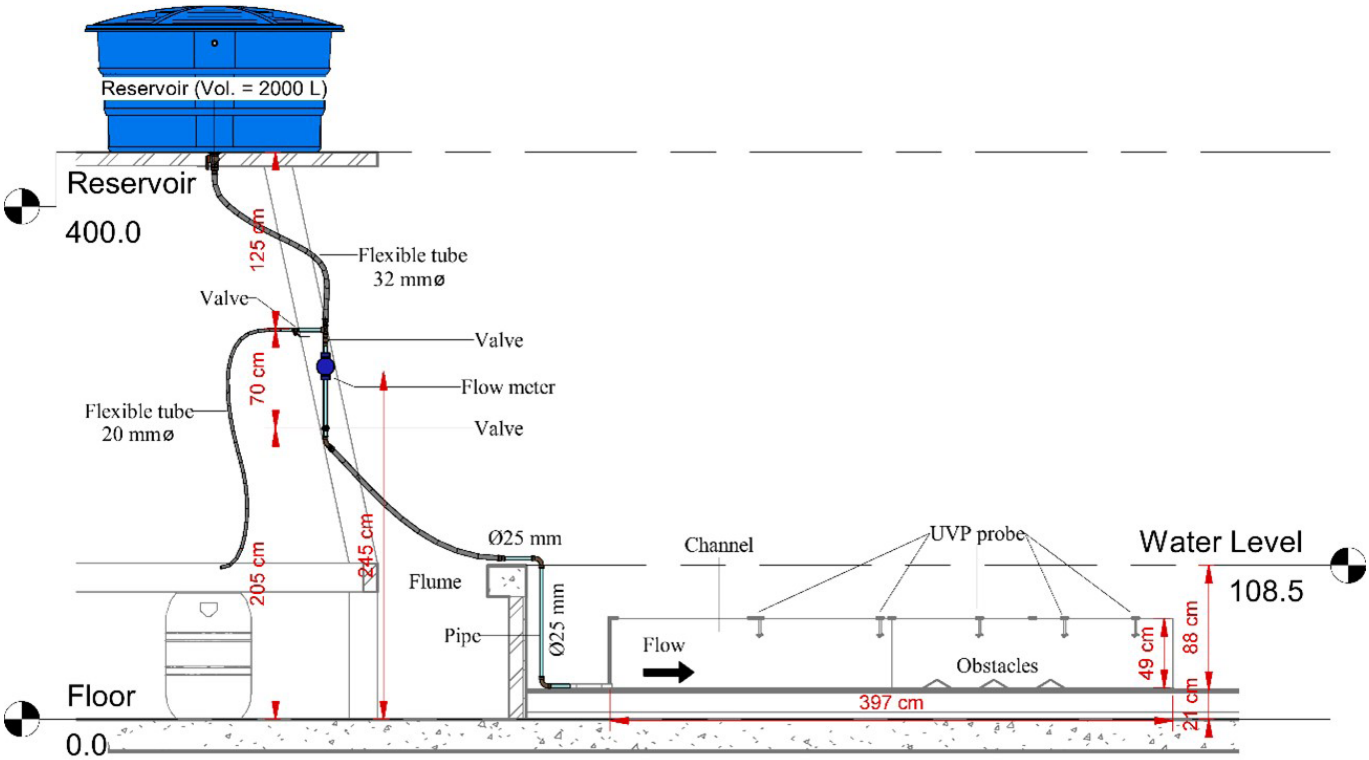

Figure 1. Lateral view of experimental apparatus.

Table 1. Predicted vs measured discharge for the runs.

Predicted discharge (L. min^{-1})	Measured (mean) Q (L. min^{-1})	Standard deviation
5	4.89	0.08
10	9.59	0.29
25	22.60	1.70

The mean value and the low standard deviation in all discharges demonstrated good control of the injected flow parameter. Only the high discharge presented a value slightly lower than predicted, without unvalidating the flow analyses.

From the data obtained with the five UVP installed along the channel, the mean velocity (U_c) in each section was calculated to verify flow development along the path. The mean velocity (U_c) was calculated considering a time-averaged data from the beginning of injection until the turbidity current stopped flowing into the channel a few minutes after cessation of injection (Figure 2). Then, the mean velocity (U_c) in each section was spatially averaged (U_{cc}) considering all five probes along the entire channel. Besides, data from thickness of flow (H_t), maximum velocity of the current (U_{max}) and height at the maximum velocity (H_{umax}) were determined from the vertical profiles of the velocity. In sequence, several parameters were calculated the mean densimetric Froude Number (Frd_{mean}) and Reynolds number (Re_{mean}). In addition, we calculated the densimetric Froude Number (Frd_{max}) and Reynolds number (Re_{max}) considering the maximum velocity (Table 2 and Table 3).

The densimetric Froude number (Frd) (Kneller & Buckee, 2000) is the ratio of inertia forces to gravitational forces, which is reduced by the density difference between the current and ambient fluid, as presented in Equation 1.

$$Frd = \frac{U_c \text{ or } U_{max}}{\sqrt{\left(\frac{\rho_c - \rho_A}{\rho_A}\right) g H_t}} \quad (1)$$

where: U_c or U_{max} mean (or maximum) velocity of the turbidity current in m.s^{-1}; g = acceleration of gravity in m.s^{-2}; H_t = height of the turbidity current in m; ρ_c = current density in kg.m^{-3}; ρ_A = density of the ambient fluid in kg.m^{-3}. The Reynolds number is the ratio of inertia forces to viscous forces, as presented in Equation 2.

$$Re = \frac{U_c \text{ or } U_{max} \cdot H_t}{\nu} \quad (2)$$

where: ν = kinematic viscosity of the mixture (m^{-2}.s) calculated by the equations presented in Castro et al. (2021).

The results show an initial deceleration after the injection point up to reaching the first obstacle. Then, the flows accelerated in the final part of the channel, regardless of the presence of obstacles. However, the flow became more intense in series 2 and 3 of runs (with obstacles) and flows of 10 and 25 L.min^{-1} (Q_2 and Q_3, respectively). The increase in the mean velocity of the flow is likely related to convective acceleration (e.g., accumulative stage *sensu* Kneller, 1995) at the center of the current (reducing its thickness) as the current exit the flume and start to spreads on the unconfined external tank (dissipation zone not evaluated here). Yet, Pohl et al. (2019) described a relaxation behavior when

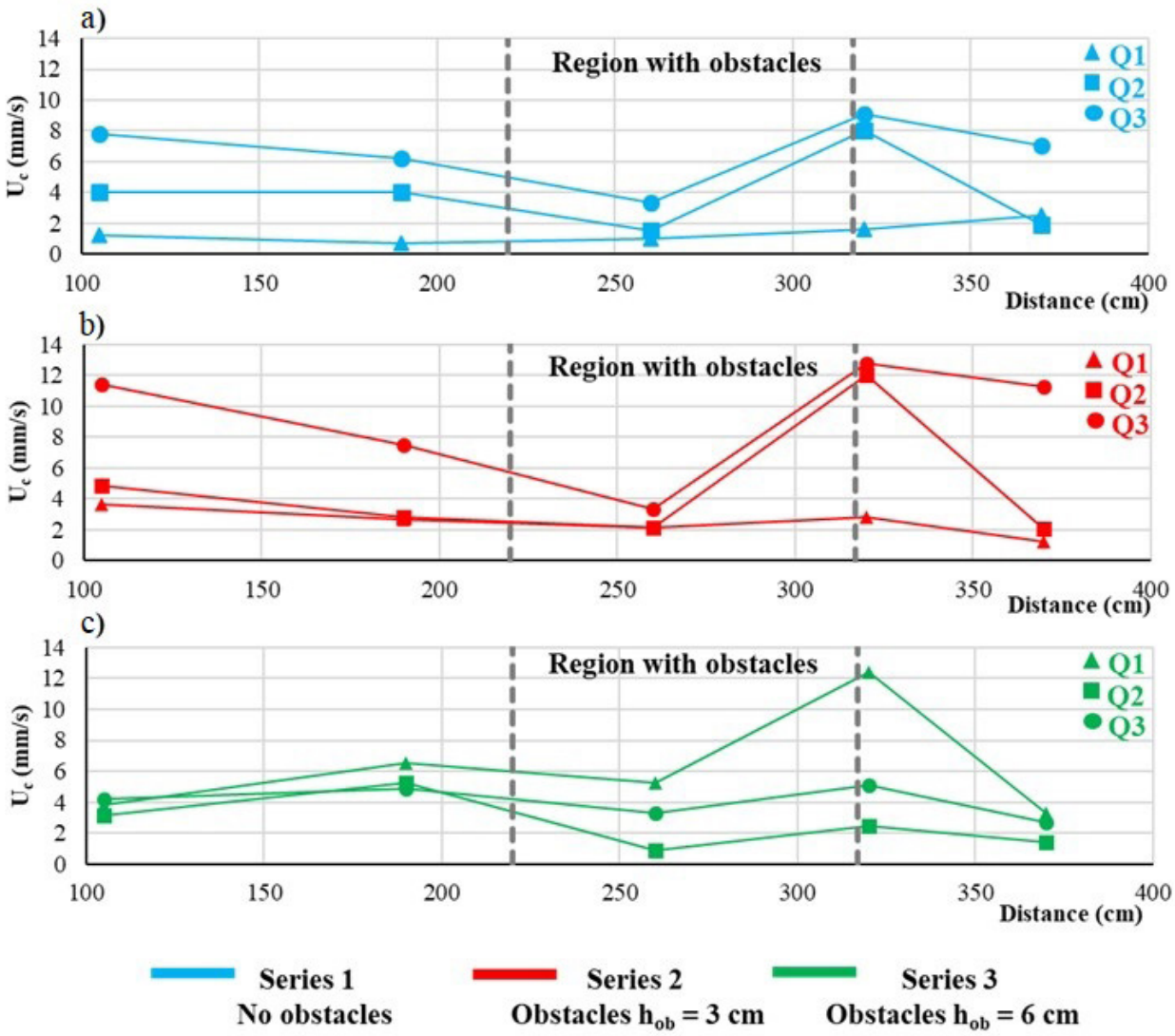

Figure 2. Turbidity current mean velocity through time averaging from injection point start to the complete dissipation of the current (U_c) at five measurement points along the channel. (a) series 1 of experiments with no-obstacles; (b) series 2 with 3-cm obstacles and; (c) series 3 with 6-cm obstacles.

Table 2. Parameters measured on the experiments runs.

Parameters	Series 1			Series 2			Series 3		
	E1.1	E1.2	E1.3	E2.1	E2.2	E2.3	E3.1	E3.2	E3.3
	No obstacles			Obstacle (h_{ob} = 3 cm)			Obstacles (h_{ob} = 6 cm)		
Q (L.min^{-1})	Q1 5	Q2 10	Q3 25	Q1 5	Q2 10	Q3 25	Q1 5	Q2 10	Q3 25
Volume Injected (L)					100				
Time of injection (min)	20	10	4	20	10	4	20	10	4
Cvol Mixt. Injected (%)	5.4	5.2	5.6	5.8	5.8	5.6	5.3	5.5	5.5
U_{cc} (mm.s^{-1})	1.4	3.9	6.7	2.5	4.8	9.3	6.3	2.6	4.0
U_{max} (mm.s^{-1})	7.7	17.6	19.8	16.3	24.4	28.1	18.5	15.6	16.8
H_t (mm)	55	85	120	50	90	130	60	90	150
H_{umax} (mm)	39	62	47	60	51	35	63	69	61
Frd_{mean}	0.01	0.03	0.04	0.02	0.03	0.05	0.06	0.02	0.02
Frd_{max}	0.07	0.13	0.12	0.15	0.17	0.17	0.16	0.12	0.09
Re_{mean}	43	222	542	83	279	784	247	158	415
Re_{max}	252	1035	1536	547	1387	2399	774	901	1590

Table 3. Time average mean velocity (U_c) and maximum velocity (U_{max}) for the five measurements points along the channel.

	Q (L.min^{-1})	H_{ob} (cm)	U_c (mm/s)					U_{max} (mm/s)				
			105 cm	190 cm	260 cm	320 cm	370 cm	105 cm	190 cm	260 cm	320 cm	370 cm
E1.1	5	-	1.20	0.68	1.03	1.61	2.52	10.09	2.43	7.01	7.24	11.71
E1.2	10	-	4.01	4.03	1.54	8.07	1.95	24.04	18.63	10.63	19.70	14.85
E1.3	25	-	7.82	6.19	3.35	9.08	7.06	25.66	17.11	9.46	23.67	23.06
E2.1	5	3	3.65	2.70	2.15	2.85	1.24	19.52	16.06	15.96	14.75	15.33
E2.2	10	3	4.87	2.81	2.14	12.01	2.10	28.79	20.04	20.02	26.19	27.01
E2.3	25	3	11.43	7.50	3.38	12.79	11.27	46.54	23.24	15.59	28.23	27.03
E3.1	5	6	3.85	6.53	5.22	12.42	3.31	18.91	18.23	13.20	28.14	14.02
E3.2	10	6	3.15	5.24	0.89	2.45	1.43	20.08	18.05	6.80	15.03	18.24
E3.3	25	6	4.22	4.88	3.31	5.10	2.68	19.63	14.59	7.89	19.85	22.30

the current gets unconfined and this process could be related to the unconfinement. However, this hypothesis needs further investigations.

The velocity profile of turbidity currents represents the ability to consolidate hydrodynamic, geometric and sedimentometric information of the turbidity current (Manica, 2012). From the velocity time series (UVP data) for each measurement point along the channel, we performed a time averaging consider the total time of the experiment (from injection until the current ceased) for the local velocity (u) in each height (z) of the current. Then, Figure 3 shows the dimensional mean vertical velocity profiles of the turbidity currents for all experiments (series 1, 2 and 3), with height (z) in millimeters and mean local velocity (u) in each height in mm.s^{-1}.

Figure 3a shows development of a "classical shape" velocity profile for diluted turbidity currents (*sensu* Altinakar et al., 1996; Kneller & Buckee, 2000; Manica, 2012), with the two regions of the flow profile and the effect of the flow jet on the upstream part also identified. The increase of discharge affects the flows with maximum velocity (nose of the current – Simpson, 1972) for higher discharges.

Figures 3b and 3c present the results considering the obstacles (yellow in the graph). We noticed the influence of the first obstacle on the shape structure of the profile after a passage of the flow (third profile from left to the right). For series 3 (h_{ob} = 6 cm), the mean velocity values present a reduction of values, indicating recirculation of the flow between these obstacles. This recirculation indicated more mixture and turbulence (green arrows on Figure 3) making the mean values constant along the vertical direction (Yaghoubi et al., 2017). For the Series 2 (h_{ob} = 3 cm), we could observe the obstacles affected the shape of the vertical profile (red arrows on Figure 3) reducing the mean values. However, the series 2 flows still present a maximum velocity nose. After the passage over the obstacles, the flows tend to regenerate in relation to their shape and magnitude displayed in the previous conditions (before obstacles), as also reported by Rossato & Alves (2011).

To help identify the effects caused by the presence of obstacles on the hydrodynamics of the current, the non-dimension velocity profiles are presented in Figure 4. The mean local velocity (u) was divided by the mean flow velocity (U_c) and the height (z) divided by the thickness of the current (H_t).

For the flow condition Q1 (5 L.min-1) (Figure 4a), the presence of obstacles (220 < x < 320 cm) resulted in non-significant effects either upstream or between the obstacles (profile x = 260 cm). However, after this point (x > 320 cm), there was a reduction in the intensity of the velocity profile, mainly for flows E3.1 (Q1 with obstacles of 6 cm).

As the discharge increases, consequently, the energy of the flow also increases. The interaction of turbidity currents with obstacles becomes more noticeable (Figures 4b and 4c). Particularly for discharge Q3 and higher obstacles (*i.e.* E3.3 – green line), strong deceleration of the flow occurs along the length of the channel (lower values compared with red and blue lines). The Figures 4b and 4c also report changes in shape of the vertical profile among the obstacles and the regeneration after passing above them (x = 320 cm and x = 370 cm), as could be seen also on Figure 3 (green arrows).

In addition, the non-dimensional profiles present similar shape distribution between experiments without obstacles and experiments with 3 cm-high obstacles (blue and red lines) for higher discharges (Figures 4b and 4c). The results suggest that the height of the obstacle causes a reduction on the non-dimensional velocity of the flows, from values around 1.0 (x < 260 cm or x > 260 cm) to values around 0.5 (x = 260 cm), but not cause significant changes in the hydrodynamic behavior of the current (shape of the profile). However, the same behaviour was not observed for lower discharges (Figure 4a), where all the three profiles showed distinct values and shapes. The Series 1 experiments (no-obstacles - blue line) presented the low-velocity values, indicating that for this less energy flows, the turbidity current decelerates thought the deposition of the particles along the flume (waning flows *sensu* Kneller, 1995). Series 2 (3 cm obstacles – red line) and Series 3 (6 cm obstacles – green line) did not show significant changes caused by the obstacles (except run 3.1 - green line at 260 cm – Figure 4a). The values and shape of the velocity profiles were alike, when we compare vertical profiles before (x < 260 cm) and after (x > 260 cm) the obstacles.

The densimetric Froude number (Equation 1) was applied as the characteristic parameter to understand the obstacle effects on the development of the turbidity current. We chose use the maximum densimetric Froude number (Frd_{max}) to better represent the locally properties of the flow, once the mean values are usually time and spaced averaged and this processes could smoothed the

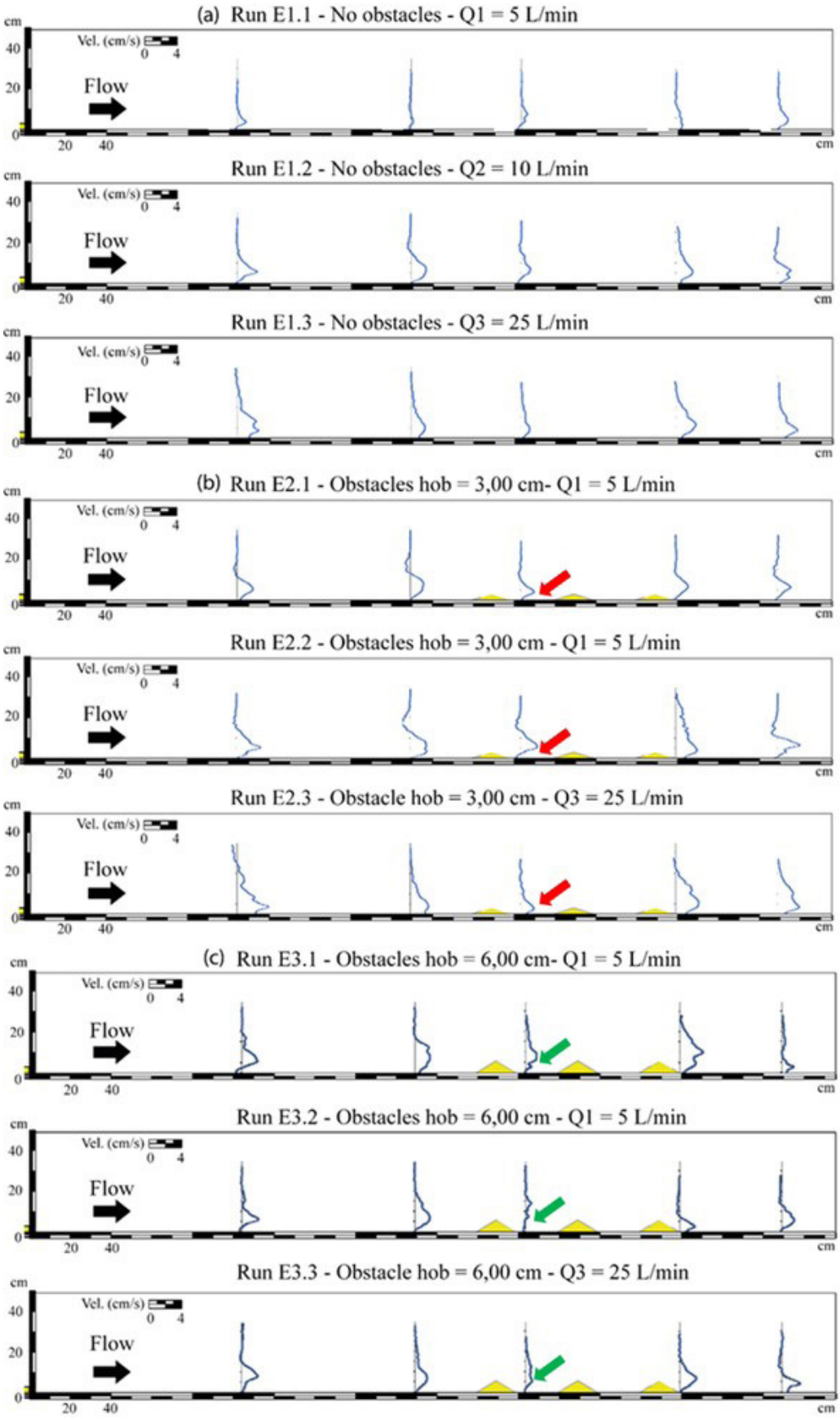

Figure 3. Mean velocity vertical profiles for each section obtained from UVP data through time averaging from injection point to the complete dissipation of the current: (a) Series 1 without any obstacles in the bed; (b) Series 2 with 3 cm obstacles; and (c) Series 3 with 6 cm obstacles.

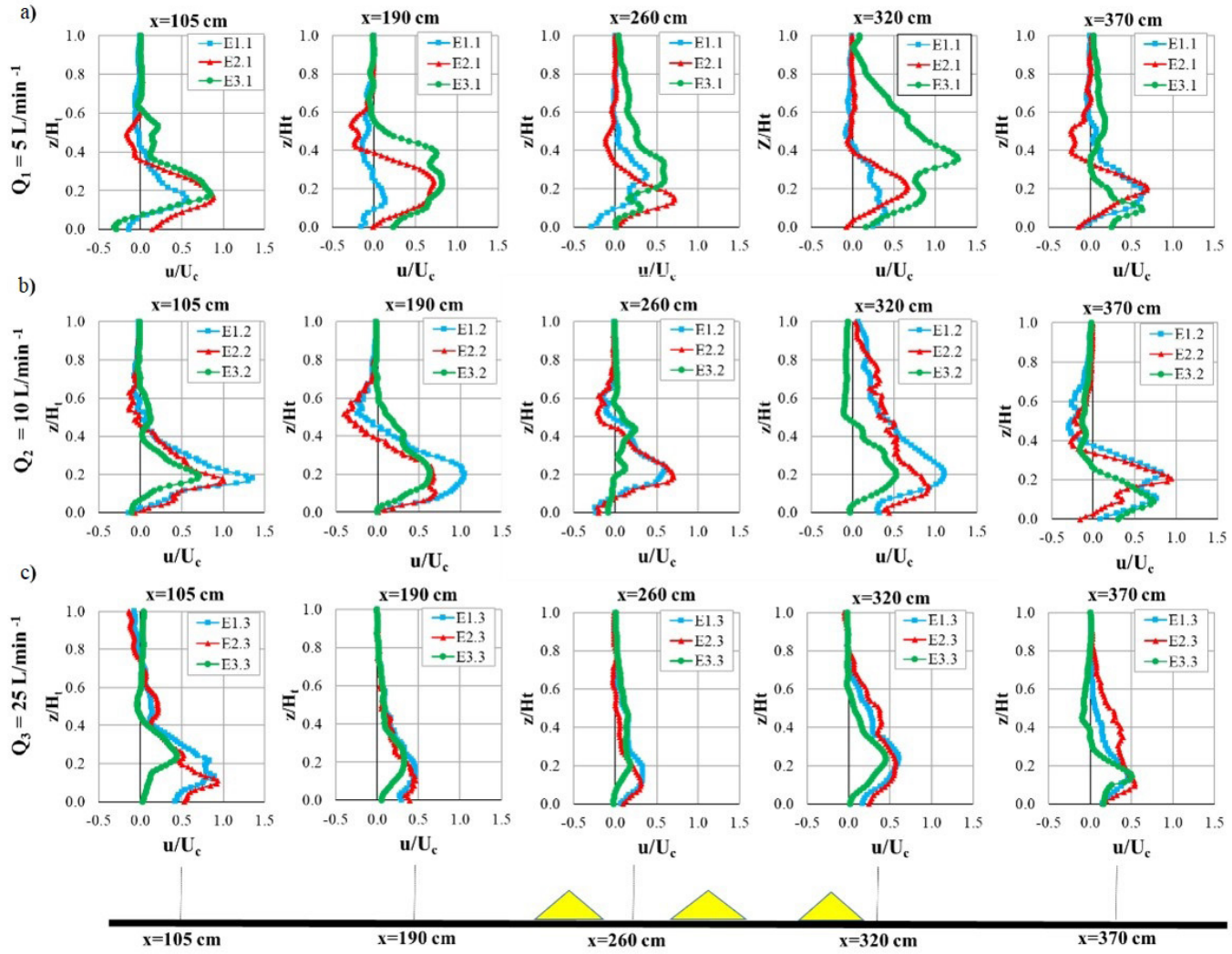

Figure 4. Non-dimensional mean velocity vertical profiles of turbidity current runs: (a) Series 1 without any obstacles in the bed (blue line); (b) Series 2 with 3 cm obstacles (red lines); and (c) Series 3 with 6 cm obstacles (green lines).

data. Figure 5 shows the maximum densimetric Froude number (Frd_{max}) values for all runs along the five measurements points of the channel.

Figure 5 consolidates the understanding that the presence of obstacles is capable of changing the hydrodynamics of the flow. The reducing maximum densimetric Froude number is observed (x ~ 260 cm) causing by reduction of mean velocity (U_c) and an increase of height (H_t). The low Frd_{max} before the obstacle, at x = 190 cm, indicates the blocking effect of flow in the first obstacle positioned at x = 220 cm (left dashed line). After the flow surpasses the obstacles, the turbidity currents tend to return to the original upstream conditions, as the maximum densimetric Froude number after the obstacle is similar to those at x = 105 cm. This behavior was also discussed by Rossato & Alves (2011) and Yaghoubi et al. (2017). However, Figure 5 do not show a clear trend on the values from no-obstacles data (blue points) to 6 cm-high obstacles data (green) in each section of the channel. The 3 cm-high obstacles (red points) presented higher values in almost all zones along the distance, while the no-obstacles (blue points) and 6 cm-high obstacles (green points) are scatter together. The same behaviour happens to the discharge marks (tringle to circle marks), as a not clear trend on the data points was observed.

In order to better visualize the individual effects of the discharge and the height of the obstacles on the entire flow, we space-average the maximum densimetric Froude number (Frd_{max}) along the channel and we related with the non-dimensionalized mean velocity by the maximum (U_c/U_{max}) for the three series of the experiments (Figure 6).

The relationship between the non-dimensional velocity (U_c/U_{max}) and the mean maximum densimetric Froude number (Frd_{max}) shows similar trends (blue and red handed fit dashed lines) of the values for the runs without obstacles (blue) and with 3 cm-high obstacles (red). The no-obstacle situation present low values comparing to the 3-cm obstacles, reinforcing the results demonstrated on Figure 5. On the other hand, the runs of the series 3 (green points and dashed line) shows a completely unlike behaviour (Figure 6a). We observed the reduction of the values from Q2 = 10 $L.min^{-1}$ to Q3 = 25 $L.min^{-1}$ (green dashed line)

similar trend to the previous series 1 (blue) and 2 (red) (apart the lower values). However, the run Q1 = 5 L.min^{-1} (green triangle marked dashed circled) not follow any trend (like an outlier point). In fact, this condition of the flow seem to suffer the presence of the 6 cm-obstacle most along the channel.

Figure 6b shows the same relationship data, however highlighting the effect of the discharge on the flows. As expected,

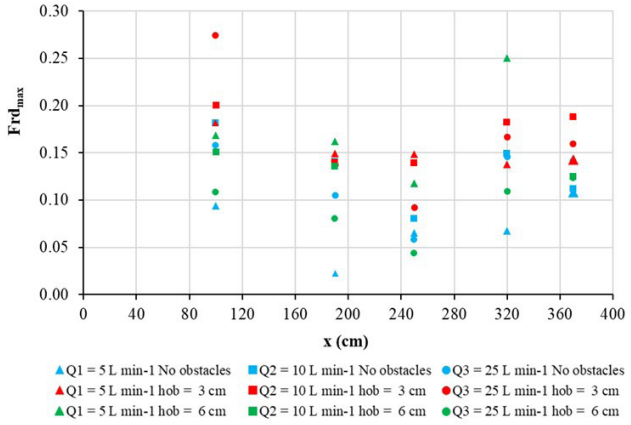

Figure 5. Maximum Densimetric Froude number (Frd$_{max}$) values for all runs along the five measurements points the channel. Dashed vertical lines indicates the region with obstacles. The colors blue, red and green indicates the series 1, 2 and 3 (from no to 6 cm obstacles). And, the triangle, square and circle marked are the discharges (from low to high).

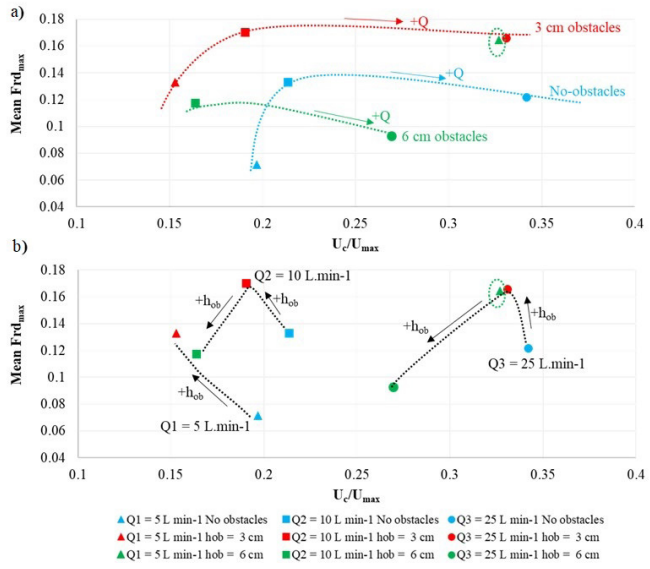

Figure 6. Relationship between the non-dimensional velocity (U$_c$/U$_{max}$) and the spaced-average maximum densimetric Froude number (Frd$_{max}$) for the three series of experiments. The colors blue, red and green indicates the series 1, 2 and 3 (from no to cm obstacles). And, the triangle, square and circle marked are the discharges (from low to high). (a) colored dashes lines were handed fit linking the same obstacles height points; (b) Black dashes lines were handed fit linking the same discharges points.

the highest discharge flows (circle points) presented the highest values of the non-dimensional velocity data, while the low discharge (triangles) the low ones. We observe the same trend lines (dashed lines) for the higher discharges Q2 = 10 L.min^{-1} (squares) to Q3 = 25 L.min^{-1} (circles), where occur an increase of the values up to height of the obstacle equal to 3 cm, and then, a reduction of the values for the 6 cm obstacles. In fact, for the high obstacles, the hydrodynamics properties of the flow were modified along the entire channel (see also Figure 4 and 5). Again, the low discharge with a high obstacle point (green triangle marked dashed circled) not follow the same trend, indicating a completely changed on the flow behaviour for that flow condition.

Figure 7 presents the relationship between the maximum densimetric Froude number (Frd$_{max}$) and the non-dimensional dimension heights (H$_{umax}$/H$_{ob}$), where H$_{umáx}$ is the height of maximum velocity.

Again, the region in the green dashed region (h$_{ob}$ = 6 cm – green points) presented the lowest maximum densimetric Froude numbers in relation to the runs with 3 cm-high obstacles (red dashed region). This result corroborates the influence of the height of the obstacle on the relationship between inertia and gravitational forces of the turbidity current. For higher obstacles, more kinetic energy of the turbidity current was converted into potential energy with the flow tending to be subcritical.

Sediment flux (q) is a parameter to verified the sediment-transport behaviour of the turbidity currents along the distance with (or not) topographic/bed alterations (i.e. obstacles). Thus, the obstacles act as flow controllers, as they have the ability to partially or totally block the turbidity current. Sediment flux (q) is calculated multiplying the mean average (U$_c$) by the thicknesses of the flow (H$_t$) and the reduced gravity $\left(\frac{\rho_C - \rho_A}{\rho_A}\right) g$. Figure 8 presents the sediment flux (q) calculated for the five measurements point along the channel, as well as, the space-averaged sediment flux (q).

According to Farizan et al. (2019), the sediment flux is strongly altered by the presence of obstacles. The Figure 8 corroborates with this, as we observed on the data at x = 260 cm, a significant

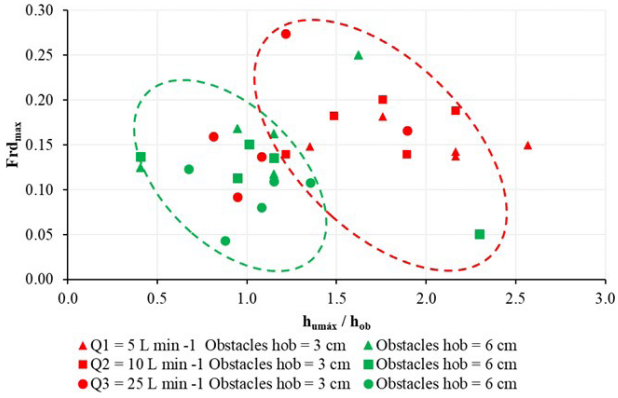

Figure 7. Relationship between the maximum densimetric Froude number (Frd$_{max}$) and maximum non-dimensional heights (H$_{umax}$/H$_{ob}$) for the two series considering obstacles. Red points are for 3 cm obstacles and green points for 6 cm obstacles.

reduction of values compared with initial position on the channel (x < 190 cm). As expected, the results indicated that turbidity currents with higher discharges (Q3) tends to transport more sediments along the channel. However, the presence of the obstacles (6 cm high obstacles – green columns) changes the hydrodynamics of the current reducing the mean sediment flux values as a considerable part of the turbidity current is partly blocked by the first obstacle. Then, the sediment flux tends to be reduced. On the other hand, the turbidity currents that flowed in the channels without obstacles (blue columns) or with obstacles of 3 cm height (red columns) suffering less resistance from the obstacles, showed similar trend of growth values of mean sediment flux (q) as also identified by Brunt et al. (2004).

DISCUSSION

The experiments performed in this work seek represents natural turbidity currents flowing over ocean basins interacting with the bed and topographic features of the sea floor (Simpson, 1987; Wynn et al., 2000; Gee et al., 2001; Parsons et al., 2007). Kneller & Buckee (2000) stated the characterization of turbidity currents through hydrodynamic parameters (e.g. velocity and concentration profile, turbulence, Richardson and densimetric Froude number) are fundamental to understand the effects of the influence of obstacles on the flow, and provides a view of cause and consequence between the hydraulics of movement and the depositional process. In this sense, the experiments carried out here sought to highlight these differences on the results present above. However, we only focused on temporal and spatial means values (Altinakar et al., 1996; Kneller, 1995; Manica, 2012), then, we could not evaluate the effects of flow turbulence itself. On the other hand, the densimetric Froude number applied on the results (Middleton, 1966; Edwards, 1993; Choux et al., 2005; Oshaghi et al., 2013; Koller, 2020), even using the maximum velocity was an enlightening parameter in order to see the effect of the obstacle in the turbidity current hydrodynamics (see Figure 5).

The effects of the densimetric Froude number of the turbidity current on obstacles have an inverse relationship with the height of current (Kneller & Buckee, 2000; Pari et al., 2010; Rossato & Alves, 2011; Oshaghi et al., 2013). This means that the effects of the obstacle are reduced as the density Froude number increases, since there is sufficient inertial energy to be transformed into potential energy, *i.e.*, to overcome the obstacles. This situation occurred in the experiments of Series 2, as the results indicated a higher densimetric Froude Number (Frd_{max}) and sediment flux (q) values, as can be seen on Figure 5 and Figure 8.

According to Oshaghi et al. (2013), turbidity currents flowing over obstacles can result in three types of behavior (Figure 9), as follows: I) turbidity currents in a subcritical state with no change in the flow regime; (IIa) partially blocked turbidity current with stationary hydraulic jump downstream of the obstacle; (IIb) turbidity current partly blocked with transient hydraulic jump downstream of the obstacle; (III) turbidity current in supercritical state without regime change; and the extreme condition of totally blocked flow.

The results presented in this work are plotted in the Oshaghi et al. (2013) diagram to check for type of turbidity current generated in the runs (Figure 9).

From Figure 9, we observe that a series of experiments with the lower height obstacles (red points) had a predominantly subcritical behavior without changing the flow regime (Figure 10a). Only experiments with Q1 = 5 L min-1 developed a relationship close to that characterized by region IIa (partially blocked turbidity current with stationary hydraulic jump downstream). The low discharge (less energy of the flow) is the main reason for this particular behavior (Kneller & Buckee, 2000; Oshaghi et al., 2013). Those results corroborate with those found in Figures 4, 6 and 8,

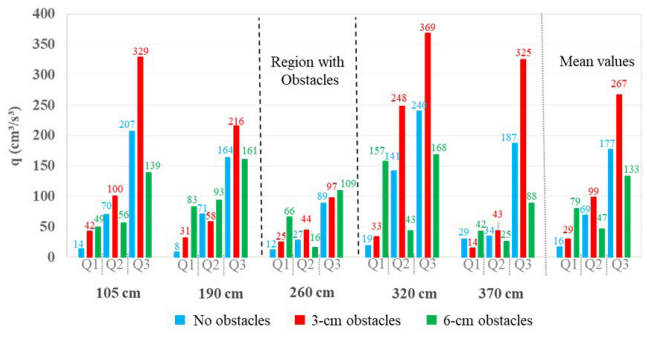

Figure 8. Sediment flux (q) calculated for the five measurements point along the channel, as well as, the space-averaged sediment flux on the right. The colors blue, red and green indicates the series 1, 2 and 3 (from no to 6 cm obstacles). Black dashed lines indicating the region with obstacles.

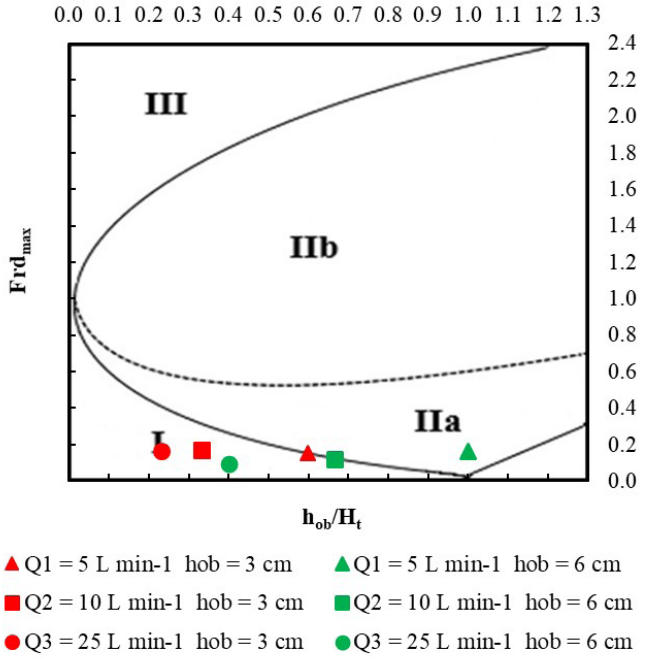

Figure 9. Relationships between the densimetric Froude number and the dimensionless height of the obstacle, according to the diagram proposed by Oshaghi et al. (2013).

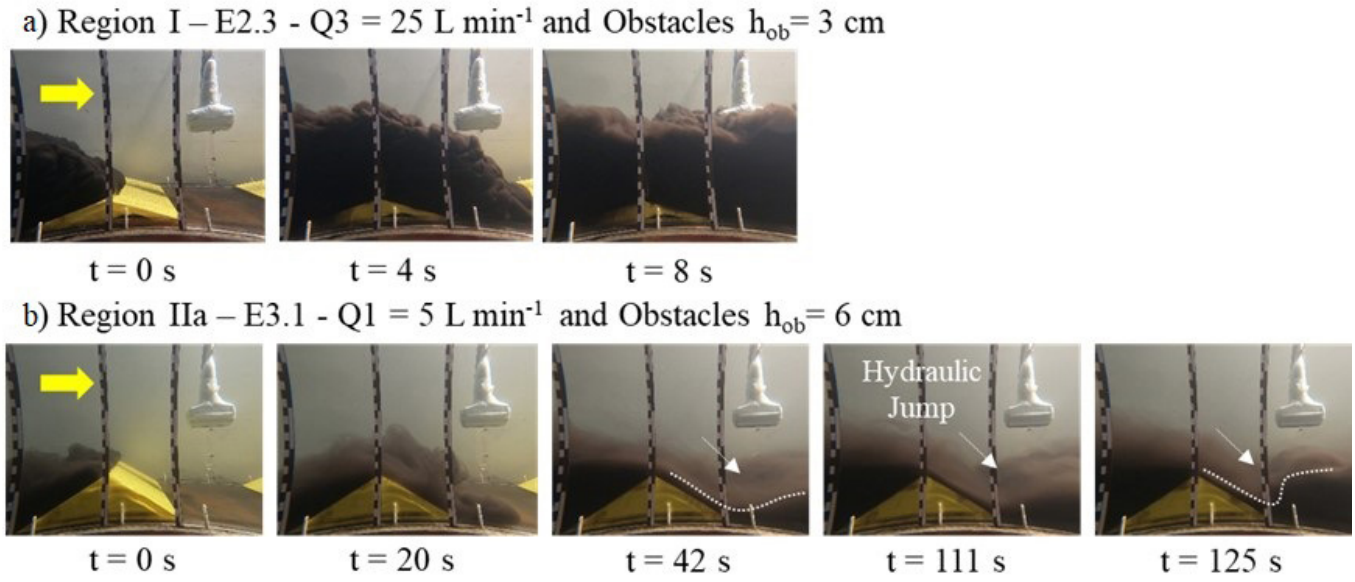

Figure 10. Images of the flow between obstacles (images taken at 220 cm from the source): (a) Subcritical Flow; (b) Partially blocked turbidity current with hydraulic jump (white dashed line). The first image considered time equal zero.

which showed close hydrodynamic behaviour of experiments with no-obstacles, that is, subcritical turbidity currents.

For runs with 6 cm-high obstacles (series 3 – green points), the behavior of turbidity currents suffered the influence of the obstacle. The Froude number was reduced (Q2 and Q3), while for the lower discharge run (Q1 - E3.1) present partially blocked with stationary hydraulic jump downstream (Figure 10b). Yet, turbidity current changed the flow regime when surpassing the obstacle from subcritical (before) to supercritical. Figure 10b displays the occurrence of a hydraulic jump (recirculation zone) modifying the typical flow structure (Komar, 1971; Tokyay et al., 2011; Yaghoubi et al., 2017), with a very thin flow over the downstream slope of the obstacle and then a thicker, turbulent roll downwards (42 s, 111 s and 125 s after the turbidity current arrived on the top of the obstacle - Figure 10b). After the passage from all three obstacles, the turbidity currents returned to the subcritical regime. This sequence occurred in all three obstacles along the channel. In addition, this recirculation could explain the outlier point (green circle dashed) present in Figure 6, that was completely away of any trend showed. The vertical profile presented on the Figure 3 and 4 also indicates the presence of recirculation between obstacles for the higher discharges (Q2 and Q3). However, only experiment Q2 (green square) are on the threshold line between regimes I and II.

The presence of obstacles acts as resistance to the flow of turbidity currents, causing the deceleration of the flow. These effects are accentuated when the obstacle is sufficient high, causing a return current similar to an open-channel flow translation wave. Concomitant to this process, the flow tends to gain energy until it overcomes the obstacle, with the critical flow occurring at the crest of the obstacle (Correia, 2012). As consequence, a partial blockage of the turbidity current occurs (Edwards, 1993; Bursik & Woods, 2000; Kubo, 2004; Correia, 2012). In our experiments, we observed evidence that the translation wave and the critical flow have acted in the experiments of the series 3 (6 cm-high obstacles), mainly in the E3.1 and E3.2 experiment (Figure 10b). The Series 3 flow parameters (e.g. velocities and Densimetric Froude number) always present lower values (see also Figures 3 to 8), not following a growing trend of values, such as showed in series 2 (3 cm-high obstacles) for instance (see Figure 6a and Figure 8). Finally, the 6 cm-high obstacles, despite 100% higher than series 2 of experiments, was unable to totally block the flow, as the flows were higher than the obstacles (Pari et al., 2010).

Regarding the flow turbulence (see also Table 2), higher flow runs (Q2 and Q3) were turbulent (Re > 500), while the lower flows indicated preponderant viscous forces (mainly E1.1). In physical modelling at the laboratory, this last behavior is predictable, because the dimensions are usually smaller (Middleton, 1966; Middleton, 1993; Paola et al., 2009, Talling et al., 2012). However, the mean velocity was calculated as time-averaged and spaced-average throughout the experiment, which may reduce the bulk Reynolds Number. Yet, at some location in the flows, e.g., proximal region and between obstacles, the turbidity currents presented higher inner turbulence (close to bottom to H_{umax} of the current).

CONCLUSIONS

The results of the controlled experiments presented here demonstrate the effect of the presence of obstacles in turbidity currents hydrodynamics. The turbidity current properties are strongly influenced by discharge and the height of the obstacles. Obstacle increase (6 cm height) leads to partially blocked flow, causing change in flow regimes (supercritical to subcritical) between obstacles. On the other hand, when the obstacle height was reduced by 50% (3 cm), turbidity current velocity developed

a behavior similar to the condition with no-obstacles. Therefore, the flow resistance of this last obstacle (3 cm high) did not lead to a significant hydrodynamic response of this interaction, and a threshold value between 3 cm and 6 cm was determined for this particular set of experiments.

The same behavior occurs with discharges. From the three values proposed, the higher discharge causes significant changes in the hydrodynamical properties and the lower discharge suffer most the effects of the obstacles. The experimental approach resulted in dimensionless relationships between the different flow parameters. Then, turbidity currents showed a reduction in the densimetric Froude number in the region between obstacles, mainly caused by the recirculation zones.

Finally, the controlled experiments performed on this work confirmed that physical modeling is a valuable tool to study physical processes. Simplifications of the runs are involved (cause-effect), but we advanced the understanding of hydrodynamic interactions between turbidity current and bed topographic features.

ACKNOWLEDGEMENTS

This research was made possible by the support and financing of Petróleo Brasileiro S.A. (Petrobras), represented by Geól. Tiago Agne de Oliveira, in partnership with UFRGS and FAURGS. We also thanks the support of the technical team of Núcleo de Estudos em Corrente de Densidade – IPH/UFRGS and Prof. Leo A. Hartmann for the English review. We are grateful to Associate Editor Iran Lima Neto, reviewer Marco Patacci, and one anonymous reviewer for their comments that led to improvement of the manuscript.

REFERENCES

Alavian, V. (1986). Behavior of density currents on an incline. *Journal of Hydraulic Engineering*, *112*(1), 27-42.

Altinakar, M. S., Graf, W. H., & Hopfinger, E. J. (1996). Flow structure in turbidity currents. *Journal of Hydraulic Research*, *34*(5), 713-718.

Brunt, R. L., McAffrey, W. D., & Kneller, B. C. (2004). Experimental modeling of the spatial distribution of grain size developed in a fill-and-spill mini-basin setting. *Journal of Sedimentary Research*, *74*(3), 438-446.

Bursik, M. I., & Woods, A. W. (2000). The effects of topography on sedimentation from particle-laden turbulent density currents. *Journal of Sedimentary Research*, *70*(1), 53-63.

Castro, C., Borges, A. L. O., & Manica, R. (2021). A new empirical viscosity model for composed suspensions used in experiments of sediment gravity flows. *Brazilian Journal of Water Resources*, *26*, e22. http://dx.doi.org/10.1590/2318-0331.262120210048.

Choux, C. M. A., Baas, J. H., McCaffrey, W. D., & Haughton, P. D. W. (2005). Comparison of spatiotemporal evolution of experimental particulate gravity flows at two different initial concentrations, based on velocity, grain size and density data. *Sedimentary Geology*, *179*(1-2), 49-69.

Correia, M. A. A. C. S. (2012). *Escoamento de correntes de turbidez sobre múltiplos obstáculos* (Dissertação de mestrado). Faculdade de Ciência e Tecnologia, Universidade Nova de Lisboa, Lisboa.

Cumberpatch, Z. A., Kane, I. A., Soutter, E. L., Hodgson, D. M., Jackson, C. A.-L., Kilhams, B. A., & Poprawski, Y. (2021). Interactions between deep-water gravity flows and active salt tectonics. *Journal of Sedimentary Research*, *91*(1), 34-65.

Edwards, D. A. (1993). *Turbidity currents: dynamics, deposits, and reversals* (Lecture Notes in Earth Sciences, No. 44, 173 p.). Berlin: Springer-Verlag.

Farizan, A., Yaghoubi, S., Firoozabadi, B., & Afshin, H. (2019). Effect of an obstacle on the depositional behaviour of turbidity currents. *Journal of Hydraulic Research*, *57*(1), 75-89.

Gee, M. J. R., Masson, D. G., Watts, A. B., & Mitchell, N. C. (2001). Passage of debris flows and turbidity currents through a topographic constriction: seafloor erosion and deflection of flow pathways. *Sedimentology*, *48*(6), 1389-1409.

Kneller, B. (1995). Beyond the turbidite paradigm: physical models for deposition of turbidites and their implications for reservoir prediction In A. J. Hartley & D. J. Prosser (Eds.), *Characterization of deep-marine clastic systems* (Special Publications, No. 94, pp. 31-49). London: Geological Society.

Kneller, B., & Buckee, C. (2000). The structure and fluid mechanics of turbidity currents: a review of some recent studies and their geological implications. *Sedimentology*, *47*, 62-94.

Koller, D. K. (2020). *Formas de fundo experimentais geradas por correntes de densidade salinas e de turbidez: análise do escoamento e do leito móvel* (Tese de doutorado). Instituto de Pesquisas Hidráulicas, Universidade Federal do Rio Grande do Sul, Porto Alegre.

Komar, P. D. (1971). Hydraulic Jumps in Turbidity Currents. *Geological Society of America Bulletin*, *82*(6), 1477-1488. http://dx.doi.org/10.1130/0016-7606(1971)82[1477:HJITC]2.0.CO;2.

Kubo, Y. (2004). Experimental and numerical study of topographic effects on deposition from two-dimensional, particle-driven density currents. *Sedimentary Geology*, *164*(3-4), 311-326. http://dx.doi.org/10.1016/j.sedgeo.2003.11.002.

Manica, R. (2009). *Geração de corrente de turbidez de alta densidade: condicionantes hidráulicos e deposicionais* (Tese de doutorado). Instituto de Pesquisas Hidráulicas, Universidade Federal do Rio Grande do Sul, Porto Alegre.

Manica, R. (2012). Sediment gravity flows: study based on experimental simulation. In H. Schulz, R. Lobosco & A. Simões (Eds.), *Hydrodynamics: natural water bodies* (Vol. 1, pp. 263-286). London: IntechOpen.

Middleton, G. V. (1966). Small-scale models of turbidity currents and the criterion for auto-suspension. *Journal of Sedimentary Petrology*, *36*, 202-208.

Middleton, G. V., & Hampton, M. A. (1973). Subaqueous sediment transport and deposition by sediment gravity flows. In D. J. Stanley, & D. J. P. Swift. *Marine sediment transport and environmental management* (pp. 197-218). New York: Wiley.

Middleton, G. V. (1993). Sediment deposition from turbidity currents. *Sediment Deposition from Turbidity Currents Annual Review of Earth and Planetary Sciences*, *21*(1), 89-114. http://dx.doi.org/10.1146/annurev.ea.21.050193.000513.

Morris, S. A., & Alexander, J. (2003). Changes in flow direction at a point caused by obstacles during passage of a density current. *Journal of Sedimentary Research*, *73*(4), 621-629. http://dx.doi.org/10.1306/112502730621.

Mulder, T., & Alexander, J. (2001). The physical character of subaqueous sedimentary density flows and their deposits. *Sedimentology*, *48*(2), 269-299. http://dx.doi.org/10.1046/j.1365-3091.2001.00360.x.

Oshaghi, M. R., Afshin, H., & Firoozabadi, B. (2013). Experimental investigation of the effect of obstacles on the behavior of turbidity currents. *Canadian Journal of Civil Engineering*, *40*, 343-352.

Paola, C., Straub, K., Mohrig, D., & Reinhardt, L. (2009). The "unreasonable effectiveness" of stratigraphic and geomorphic experiments. *Earth-Science Reviews*, *97*(1-4), 1-43. http://dx.doi.org/10.1016/j.earscirev.2009.05.003.

Pari, S. A. A., Kashefipour, S. M., Ghomeshi, M., & Bajestan, M. S. (2010). Effects of obstacle heights on controlling turbidity currents with different concentrations and discharges. *Journal of Food Agriculture and Environment*, *8*(2), 930-935.

Parsons, J. D., Friedrichs, C. T., Traykovski, P. A., Mohrig, D., Imran, J., Syvitski, J. P. M., Parker, G., Puig, P., Buttles, J. L., & García, M. H. (2007). The mechanics of marine sediment gravity flows. In C. Nittrouwer, J. Austin, M. Field, J. Syvitski & P. Wiberg (Eds.), *Continental margin sedimentation: from sediment transport to sequence stratigraphy* (Special Publication IAS, pp. 275-337). Malden: Blackwell Publishing.

Patacci, M., Haughton, P., & McCaffrey, W. (2015). Flow behavior of ponded turbidity currents. *Journal of Sedimentary Research*, *85*(8), 885-902. http://dx.doi.org/10.2110/jsr.2015.59.

Pohl, F., Eggenhuisen, J. T., Tilston, M., & Cartigny, M. J. B. (2019). New flow relaxation mechanism explains scour fields at the end of submarine channels. *Nature Communications*, *10*(1), 4425. http://dx.doi.org/10.1038/s41467-019-12389-x.

Rossato, R., & Alves, E. (2011). Experimental study of turbidity currents flow around obstacles. In *Proceedings of the 7th International Symposium on Stratified Flows*, Rome, Italy.

Simpson, J. E. (1969). A comparison between laboratory and atmospheric density currents. *Quarterly Journal of the Royal Meteorological Society*, *95*(406), 758-765. http://dx.doi.org/10.1002/qj.49709540609.

Simpson, J. E. (1972). Effects of the lower boundary on the head of a gravity current. *Journal of Fluid Mechanics*, *53*(4), 759-768. http://dx.doi.org/10.1017/S0022112072000461.

Simpson, J. E. (1987). *Gravity currents: in the environment and the laboratory*. Devon: Ellis Horwood Ltd.

Talling, P. J., Masson, D. G., Sumner, E. J., & Malgesini, G. (2012). Subaqueous sediment density flows: depositional processes and deposit types. *Sedimentology*, *59*(7), 1937-2003. http://dx.doi.org/10.1111/j.1365-3091.2012.01353.x.

Tokyay, T., Constantinescu, G., Gonzalez-Juez, E., & Meiburg, E. (2011). Gravity currents propagating over periodic arrays of blunt obstacles: effect of obstacle size. *Journal of Fluids and Structures*, *27*(5-6), 798-806. http://dx.doi.org/10.1016/j.jfluidstructs.2011.01.006.

Wynn, R. B., Masson, D. G., Stow, D. A., & Weaver, P. P. (2000). The northwest African slope apron: a modern analogue for deep-water systems with complex seafloor topography. *Marine and Petroleum Geology*, *17*(2), 253-265. http://dx.doi.org/10.1016/S0264-8172(99)00014-8.

Yaghoubi, S., Afshin, H., Firoozabadi, B., & Farizan, A. (2017). Experimental investigation of the effect of inlet concentration on the behavior of turbidity currents in the presence of two consecutive obstacles. *Journal of Waterway, Port, Coastal, and Ocean Engineering*, *143*(2), 04016018. http://dx.doi.org/10.1061/(ASCE)WW.1943-5460.0000358.

Authors contributions

Arthur Costa Cerqueira: Idealization of the scope of work, planning, execution and interpretation of experimental data.

Rafael Manica: Orientation in decisions, as well as in idealizing the scope of work, in planning, execution and interpretation of experimental data.

Editor-in-Chief: Adilson Pinheiro

Associated Editor: Iran Eduardo Lima Neto